

Electronic Supplementary Information

Graphdiyne: A Superior Carbon Additive to Boost Water Oxidation Catalyst

Panyong Kuang,^a Bicheng Zhu,^a Yuliang Li,^c Huibiao Liu,^c Jiaguo Yu^{*ab} and
Ke Fan^{*a}

^aState Key Laboratory of Advanced Technology for Materials Synthesis and Processing,
Wuhan University of Technology, Wuhan 430070, P. R. China

^bDepartment of Physics, Faculty of Science, King Abdulaziz University, Jeddah 21589,
Saudi Arabia

^cBeijing National Laboratory for Molecular Sciences (BNLMS), CAS Key Laboratory of
Organic Solids, Institute of Chemistry, Chinese Academy of Sciences, Beijing 100190, P.
R. China

Tel: 0086-27-87871029; Fax: 0086-27-87879468

E-mail: jiaguoyu@yahoo.com; kefan@whut.edu.cn

Experimental

Materials and Chemicals

Hexabromobenzene was obtained from J&K Scientific. Tetrabutylammonium fluoride (TBAF) was purchased from Alfa Aesar. Tetrahydrofuran (THF) was pretreated by drying under reflux with Na crumbs. $\text{NiSO}_4 \cdot 6\text{H}_2\text{O}$, $\text{FeSO}_4 \cdot 7\text{H}_2\text{O}$, $\text{CH}_4\text{N}_2\text{O}$ (urea), $\text{Na}_3\text{C}_6\text{H}_5\text{O}_7 \cdot 2\text{H}_2\text{O}$ (trisodium citrate) and KOH were provided by Sinopharm Chemical Reagent Co., Ltd. Commercial RuO_2 was purchased from Aladdin Industrial Corporation. Nafion (5 wt %, ethanol solution) was provided by Yi Er Sheng (Kunshan) International Trade Co. Ltd. Graphite and carbon nanotubes were purchased from The Six Element (Changzhou) Materials Technology Co., Ltd. and Cnano (Zhenjiang) Technology Co., Ltd., respectively.

Synthesis of GDY/NiFe-LDH

Bulk GDY film was first prepared on the surface of copper using a modified Glaser-Hay coupling reaction using hexaethynylbenzene (HEB) precursors, as described previously.¹ The resulting bulk GDY film was exfoliated under sonication for several weeks to form a homogeneous aqueous dispersion of GDY, and then dried to collect the powders. As for the synthesis of GDY/NiFe-LDH, 4.0 mg of GDY was dispersed in 20 mL of mixed solution containing 1.0 mmol $\text{NiSO}_4 \cdot 6\text{H}_2\text{O}$, 0.33 mmol $\text{FeSO}_4 \cdot 7\text{H}_2\text{O}$, 2.8 mmol urea and 0.11 mmol trisodium citrate, which was blended by vigorous stirring for 30 min and sonication for 30 min. After that, the solution was transferred into a 30 mL Teflon-lined stainless steel autoclave and hydrothermally treated at 180 °C for 12 h. The final products were collected by centrifugation, and washed by deionized water and ethanol for several times. To obtain the optimal OER performance of GDY/NiFe-LDH, a number of control samples with varied GDY weight ratio were synthesized.

Synthesis of RGO/NiFe-LDH and CNT/NiFe-LDH

Firstly, GO was prepared by modified Hummer's method.² In a typical procedure, a certain amount of graphite powder was first stirred in 23 mL of concentrated sulfuric acid at 45 °C for 24 h. Then, 0.1 g of NaNO_3 was added into the above solution with continuous stirring at 45 °C for 5 min. After being cooled in an ice-water bath, 3 g of KMnO_4 was gradually added to form a new mixture. Then, appropriate amount of deionized water was poured into the solution with continuous stirring at 90 °C for 15 min. Finally, 140 mL of deionized water and 10 mL H_2O_2 were added into the solution after cooling to room temperature and stirred for another 10 min. The resulted mixture solution was washed by HCl (10 vol %) solution and deionized water for several times, then the precipitates were collected by centrifugation. Finally, the

collected products were re-dispersed in deionized water to form the GO homogeneous solution. As for the synthesis of RGO/NiFe-LDH and CNT/NiFe-LDH, similar methods were conducted except GDY was replaced by GO and CNT, respectively. After hydrothermal treatment, the GO was reduced to RGO.³ The final products were collected by centrifugation, and washed by deionized water and ethanol for several times.

Characterizations

SEM and EDS (JEOL JSM-7500) measurements were used to examine the surface morphology and elements of samples. The microstructure of the sample was investigated by TEM (JEOL JEM-2100F). ACTEM and HAADF were performed by FEI Titan G2 60-300 instrument. The surface image and roughness of GDY film and NiFe-LDH nanoplate was conducted on multimode 8 AFM (Bruker, USA) in tapping mode. XRD was conducted by using Rigaku diffractometer (Japan) equipped with monochromatized Cu K α radiation ($\lambda = 0.15418$ nm). The TG-DTA curve was performed on a DTG-60H analyzer (Shimadzu Corp., Tokyo, Japan) under air condition with a heating rate of 5 °C min⁻¹. XPS was performed through a Thermo XPS spectrometer system (ESCALab 250) using Al K α (1486.6 eV, 150 W) radiation. Raman spectroscopy was performed using RenishawinVia spectrometer ($\lambda = 514.5$ nm) at room temperature. The FT-IR analyses were performed using a Nicolet iS50 FT-IR spectrometer (Thermo). The contents of Ni and Fe elements were examined by ICP-AES measurement.

Electrode Preparation

2.0 mg of the catalysts and 10 μ L of 5 wt % Nafion were dispersed in a mixture solution comprising of 250 μ L H₂O and 250 μ L ethanol. After the constant sonication for 20 min, 5.0 μ L of the homogeneous ink was dropped onto the pre-polished glassy carbon electrode (GCE, diameter: 3 mm, area: 0.07 cm²), and then dried naturally at room temperature.

Electrochemical Measurements

All of the electrochemical performances were investigated using an electrochemical workstation (CHI 760E, Chenhua, Shanghai) with the catalysts modified GCE as the working electrode, Pt plate as the counter electrode, and Hg/HgO (1.0 M KOH) electrode as the reference electrode. 1.0 M aqueous KOH served as the electrolyte for OER activity test. All measured potentials were converted to the reversible hydrogen electrode (RHE) using the Nernst equation below:⁴

$$E_{\text{RHE}} = E_{\text{Hg/HgO}} + 0.059\text{pH} + E^{\ominus}_{\text{Hg/HgO}}$$

where the E_{RHE} is the converted potential vs. RHE, $E_{\text{Hg/HgO}}$ is the applied potential vs. Hg/HgO reference electrode, and $E^0_{\text{Hg/HgO}}$ is the standard potential of Hg/HgO electrode at 25 °C (0.097 V). Overpotential (η) = $E_{\text{RHE}} - 1.23$ V. Before the OER test, CV was performed from -0.42 to 0.98 V vs. Hg/HgO at a scan rate of 100 mV s⁻¹ for 60 cycles to clean and activate the GCE. After CV activation, polarization curves were obtained by linear sweep voltammetry (LSV) from 0.28 to 0.78 V vs. Hg/HgO with a scan rate of 5 mV s⁻¹ in 1.0 M KOH solution, and corrected by iR compensation. Nyquist plots were collected in a frequency range of 100 KHz to 0.1 Hz with AC voltage amplitude of 10 mV at 1.53 V vs. RHE. For the long-term durability test, static overpotential and current density were fixed for a certain time during continuous OER process to obtain the time-dependent current density and overpotential, respectively. The ECSA of samples were measured through double-layer charging (C_{dl}) from CV with different scan rate (20 – 120 mV s⁻¹). The C_{dl} of samples were estimated by plotting the $\Delta J = J_a - J_c$ against CV scan rate, where the slope value was twice of C_{dl} and can be used to represent the ECSA. The value of TOF was estimated by assuming that all metal sites (Ni and Fe) are actively involved in the electrocatalysis:⁵

$$\text{TOF} = JAn^{-1}F^{-1}m^{-1}$$

where J (mA cm⁻²) denotes the current density at a given overpotential, A is the surface area of the working electrode (0.07 cm²), n denotes the electron transfer number ($n = 4$ for OER), F is the Faraday constant (96485 s A mol⁻¹), and m is the total mole number of the metals.

Characterization after Long-term Stability Test:

Generally, the characterization after stability test is very hard because of the small amount of catalysts on GCE and the Nafion in catalysts suspension. In this regard, a catalysts suspension was prepared through the same approach described above but without adding Nafion solution, then a relatively large amount of suspension was dropped onto a clean F-doped SnO₂ (FTO) glass substrate (active surface area: 4 cm²) and used as working electrode. The catalysts on FTO glass after test were used for further characterization.

DFT Calculations

The DFT calculations were conducted by using the VASP code. The exchange-correlation interaction was described by generalized gradient approximation (GGA) with the Perdew-Burke-Ernzerhof (PBE) functional. The energy cutoff and Monkhorst-Pack k-point mesh were set to be 400 eV and 3 × 3 × 1, respectively. During the geometry optimization, the convergence tolerance was set as 1.0 × 10⁻⁴ eV for energy. For the construction of surface models, a vacuum of 20 Å was used to eliminate

interactions between periodic structures. The DFT-D2 method of Grimme was employed to treat the van der Waals (vdW) interaction.

To achieve the lattice match between GDY, RGO and NiFe-LDH, 1×1 primitive cell of GDY, 4×4 supercell of RGO and 3×3 supercell of NiFe-LDH were used. After geometry optimization, the lattice parameters are $a = b = 9.45 \text{ \AA}$ for GDY, $a = b = 9.87 \text{ \AA}$ for RGO, $a = 9.47 \text{ \AA}$ and $b = 9.44 \text{ \AA}$ for NiFe-LDH. The lattice mismatch between GDY and NiFe-LDH is only 0.2%, and that between RGO and NiFe-LDH is smaller than 4.5%. The NiFe-LDH model consists of four layers of metal hydroxides. The metal atoms in the second layer are Fe atoms and those in other three layers are Ni atoms, thus forming the Ni/Fe molar ratio of 3/1 in NiFe-LDH. Moreover, the adhesive energy (E_a) is defined as $E_a = E_{\text{LDH/C}} - E_{\text{LDH}} - E_C$, where E_{LDH} is the energy of NiFe-LDH, E_C is the energy of GDY or RGO, $E_{\text{LDH/C}}$ is the energy of GDY/NiFe-LDH or RGO/NiFe-LDH.

Moreover, the work function (Φ) was calculated using the following equation:⁶

$$\Phi = E_{\text{vac}} - E_F$$

where E_F is the Fermi level energy, E_{vac} is the electrostatic potential of the vacuum level.

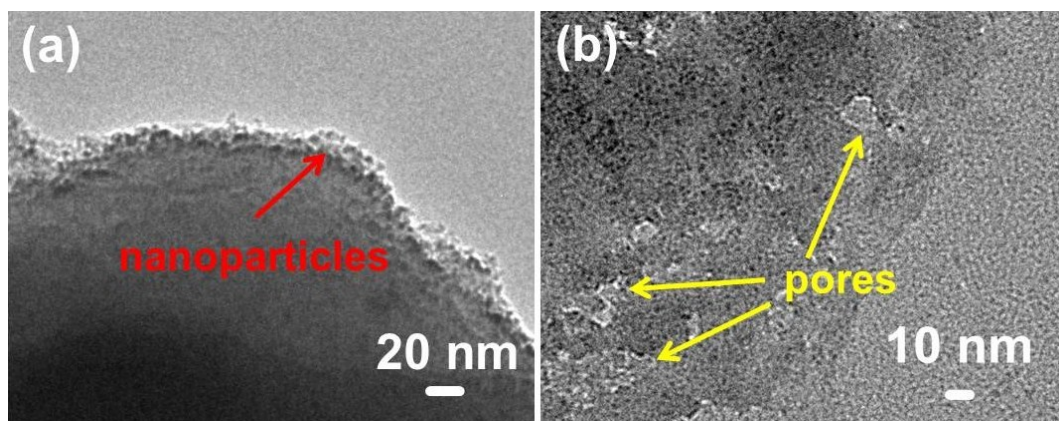


Fig. S1. (a) The graininess and (b) porous structure of GDY.

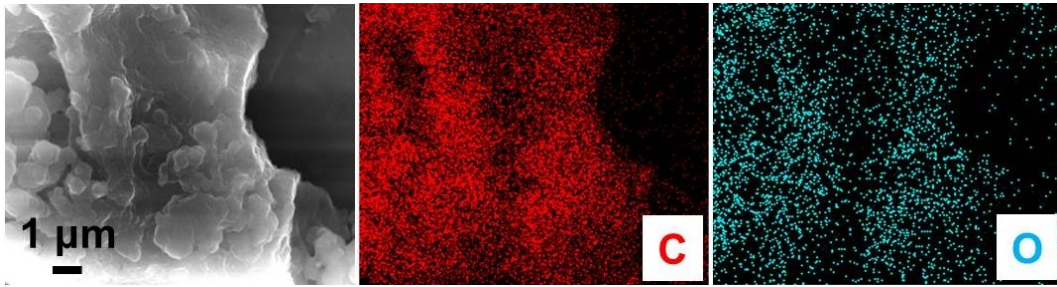


Fig. S2. EDS mapping images of the GDY

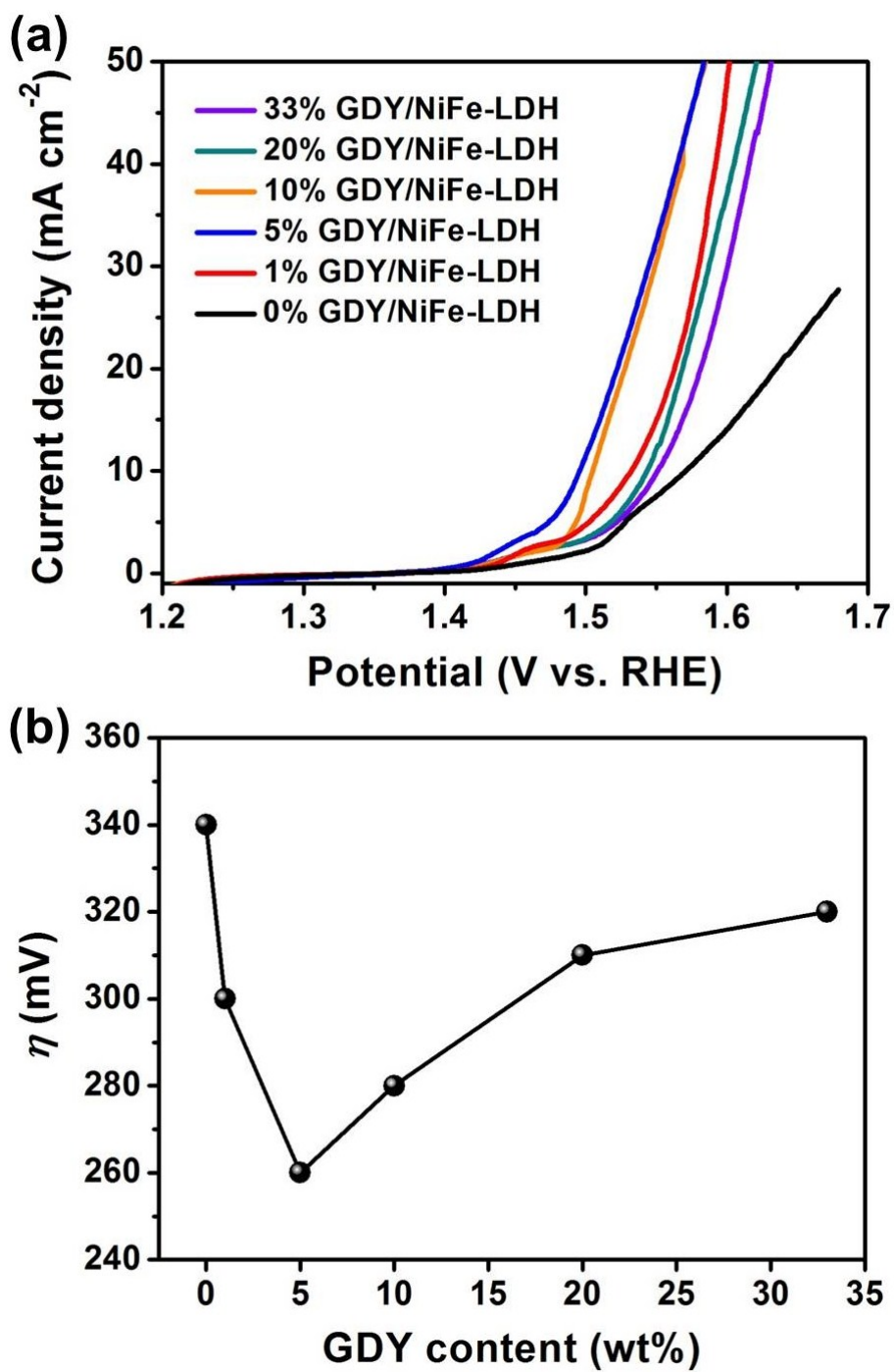


Fig. S3. (a) Polarization curves and (b) overpotential at 10 mA cm⁻² obtained on GDY/NiFe-LDH electrocatalysts with different GDY mass percentage.

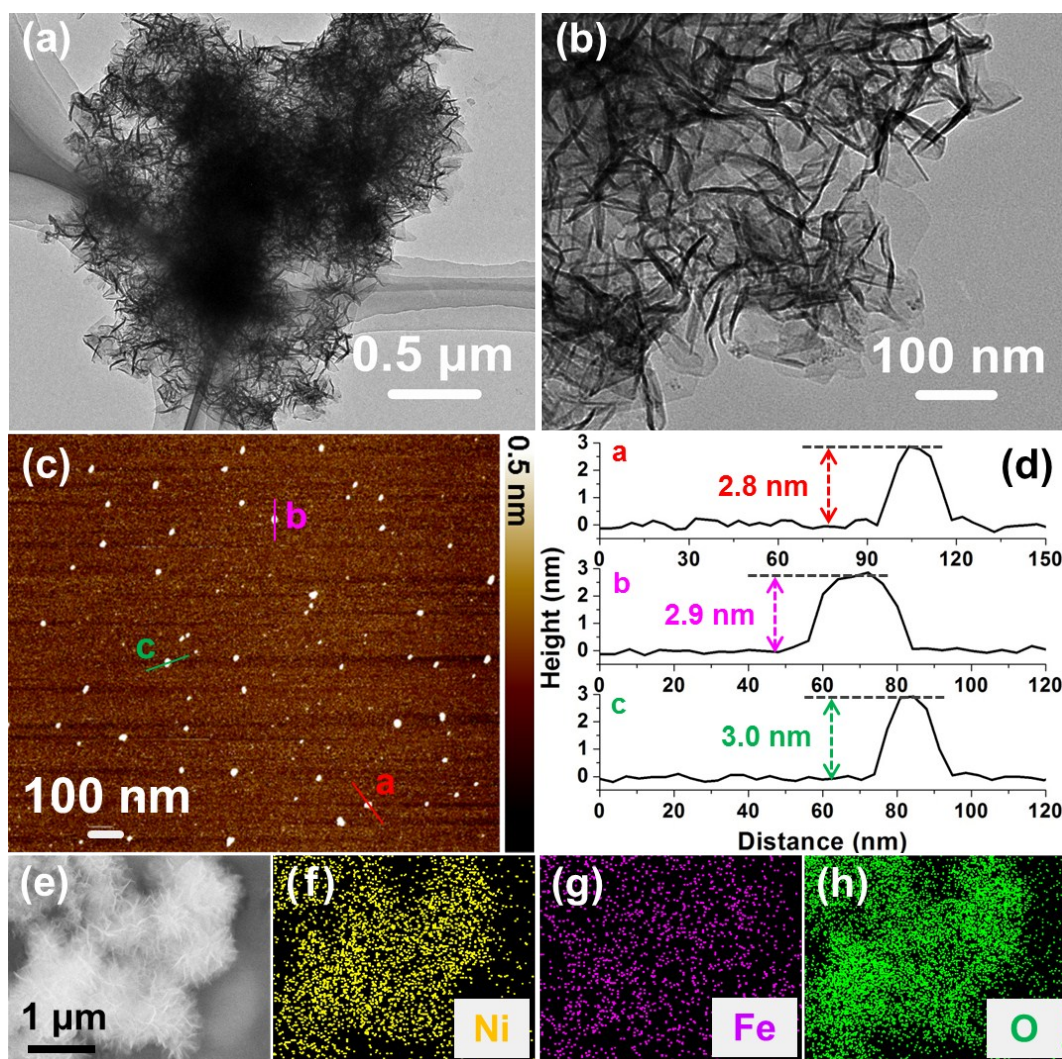


Fig. S4. (a and b) TEM images, (c and d) AFM image and (e-h) EDS mapping images of NiFe-LDH.

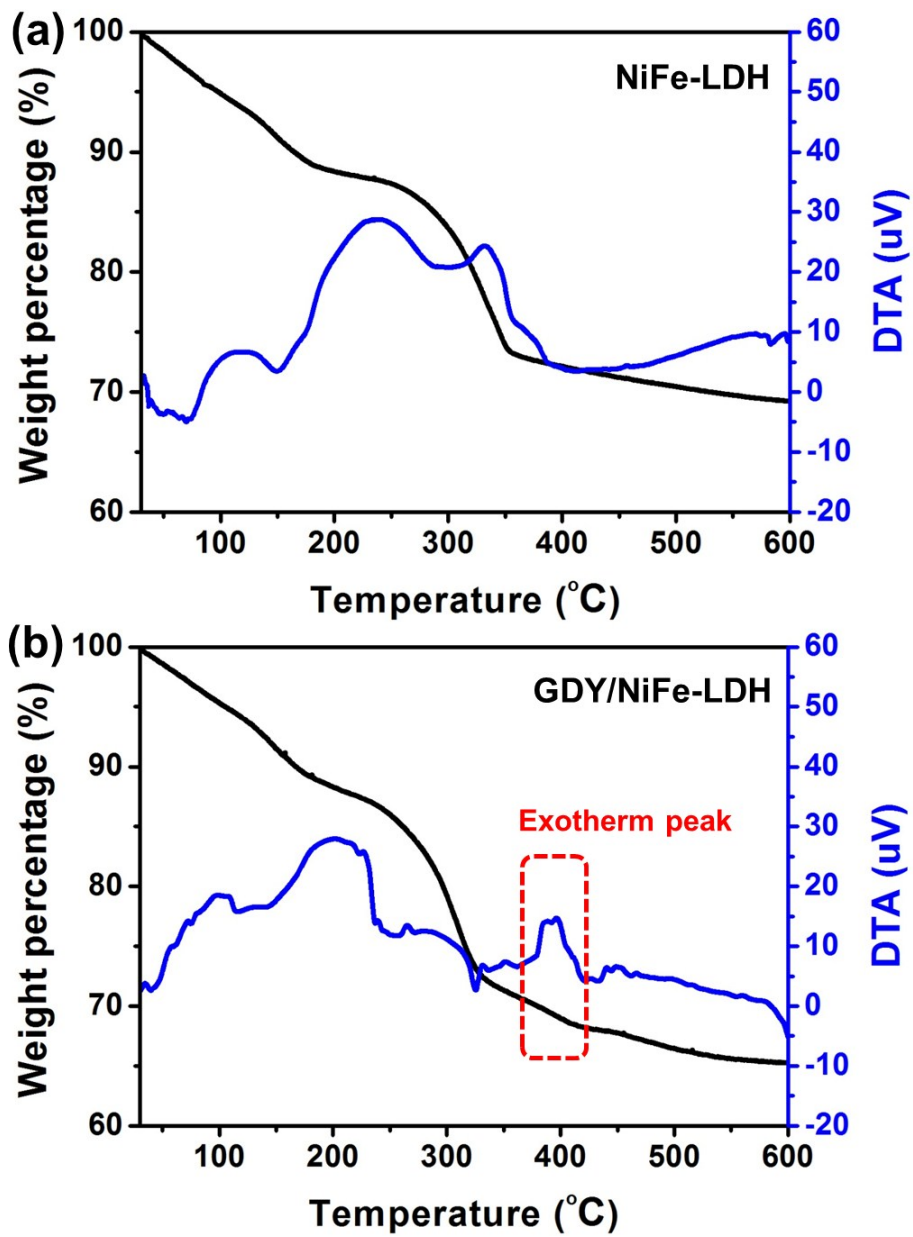


Fig. S5. TG and DTA curves of (a) NiFe-LDH and (b) GDY/NiFe-LDH.

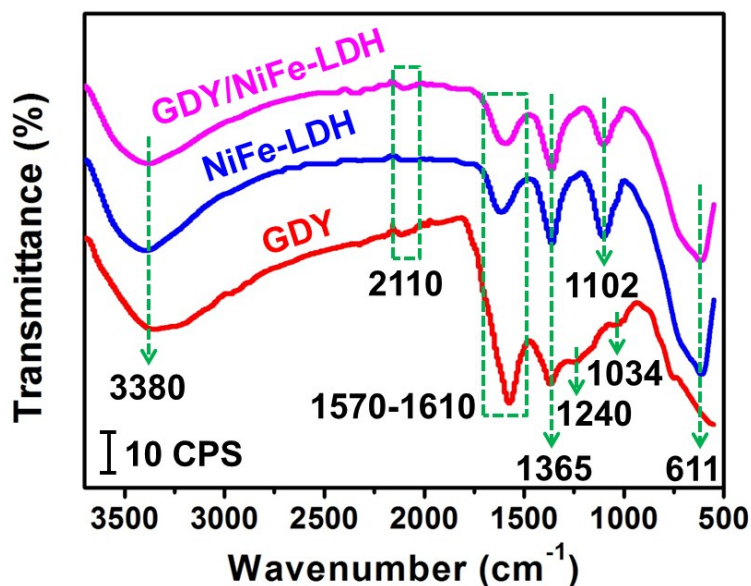


Fig. S6. FT-IR spectra of GDY/NiFe-LDH, NiFe-LDH and GDY.

The broad and strong absorbance peak at about 3380 cm^{-1} is related to the stretching vibration of O-H band of the hydroxide layers and interlayer water.⁷ The band at 2110 cm^{-1} is the typical $\text{C}\equiv\text{C}$ stretching vibration, and its slightly weak intensity is attributed to the molecular symmetry.⁸ The band located at 1570 cm^{-1} for GDY is assigned to the skeletal vibration of aromatic rings, and the band located at 1610 cm^{-1} for NiFe-LDH is assigned to -OH groups in the interlayer water.⁸ Therefore, the band at 1600 cm^{-1} for GDY/NiFe-LDH is attributed to the synergistic results of aromatic rings and water molecules. The band located at 1365 cm^{-1} may be ascribed to the vibration of hydroxyls attached to carbon (C-OH) for GDY and interlayer carbonate (CO_3^{2-}) of NiFe-LDH.⁹⁻¹¹ The bands centered at 1240 and 1034 cm^{-1} of GDY can be indexed to the stretching vibrations of carboxyl C-O bonds and epoxy C-O-C bonds, respectively.¹² In addition, the bands at around 1102 and 611 cm^{-1} of NiFe-LDH and GDY/NiFe-LDH can be attributed to the sulfates and metal-hydrogen/metal-oxygen bonds, respectively.¹³

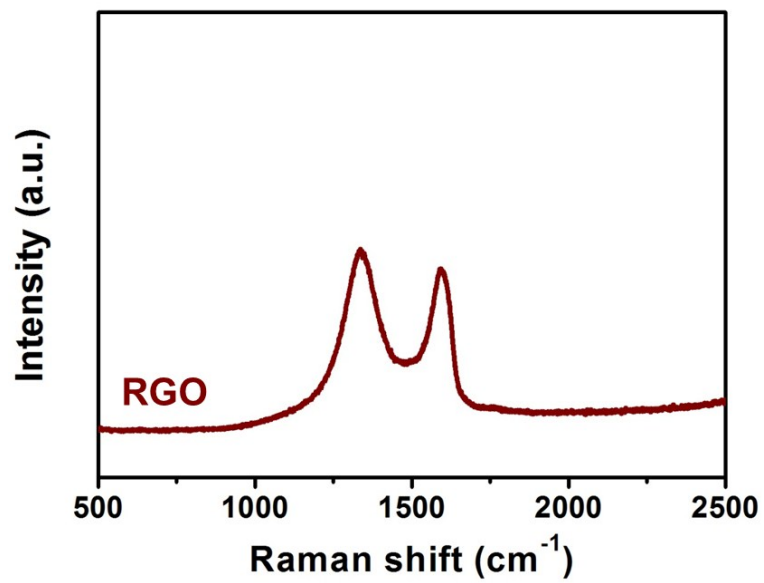


Fig. S7. Raman spectrum of the RGO.

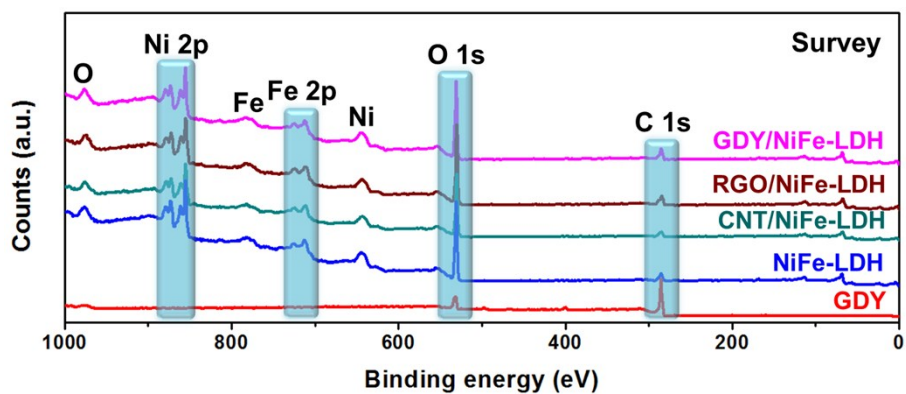


Fig. S8. XPS survey spectra of GDY/NiFe-LDH, RGO/NiFe-LDH, CNT/NiFe-LDH, NiFe-LDH and GDY.

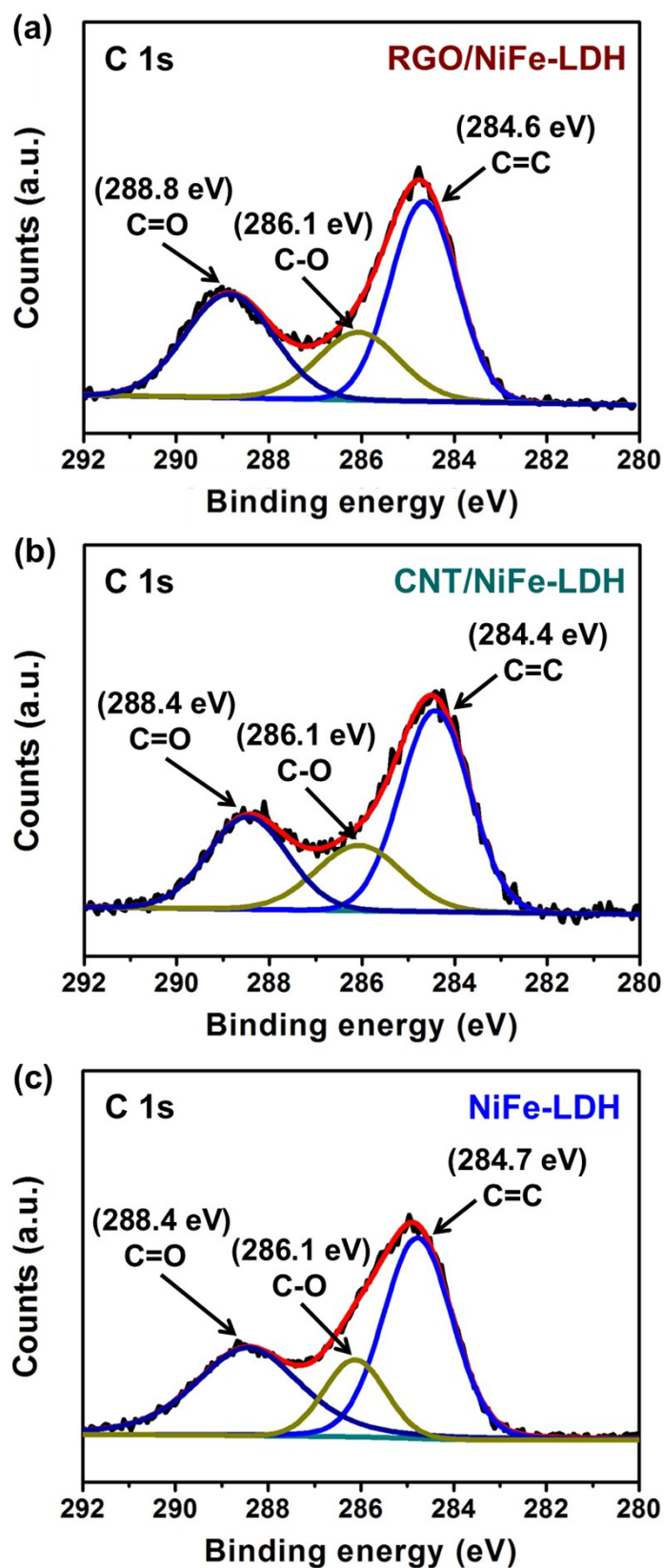


Fig. S9. C 1s XPS spectra of (a) RGO/NiFe-LDH, (b) CNT/NiFe-LDH and (c) NiFe-LDH.

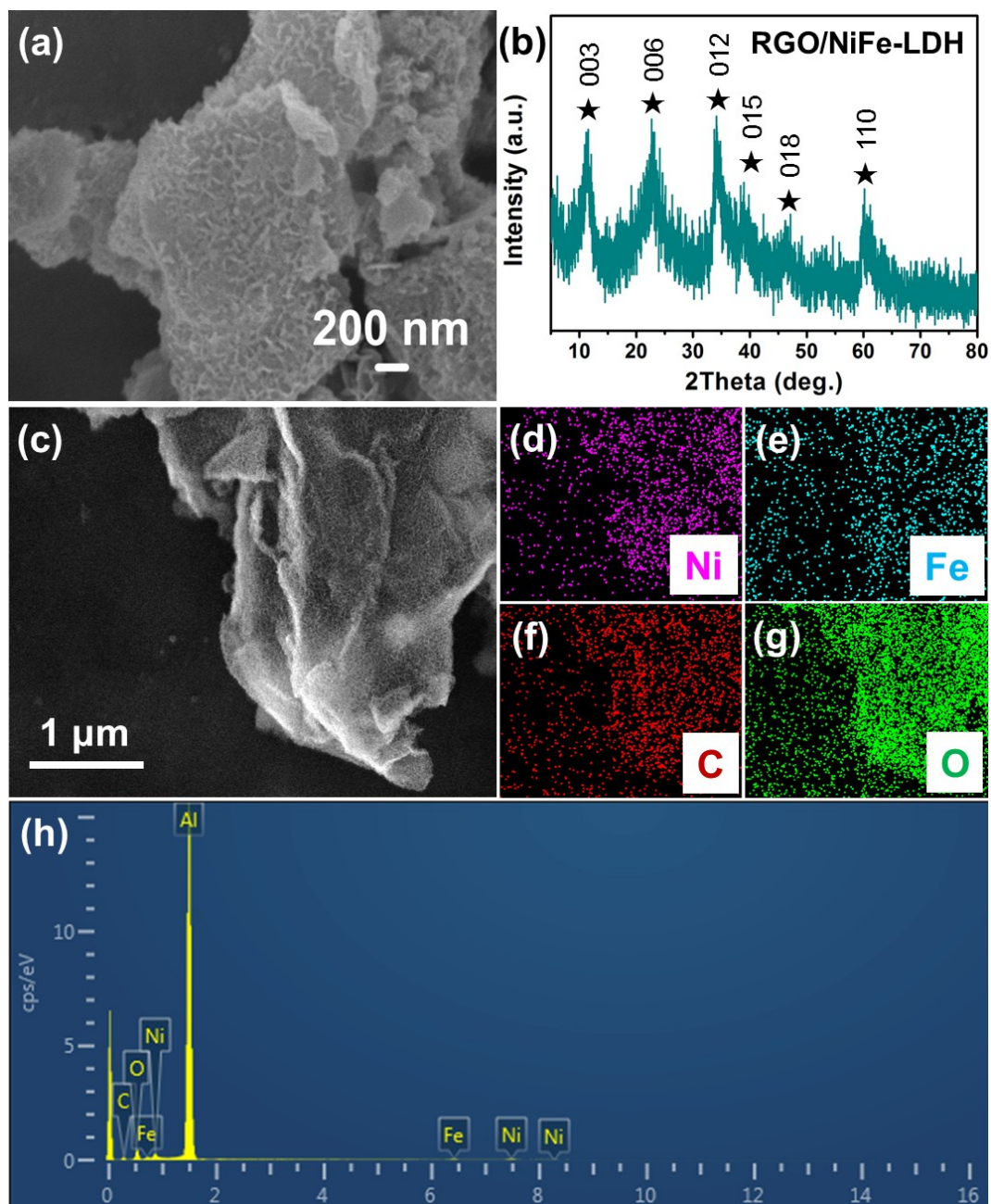


Fig. S10. (a and c) SEM images, (b) XRD pattern, and (d-h) corresponding EDS mapping images of the RGO/NiFe-LDH counterpart.

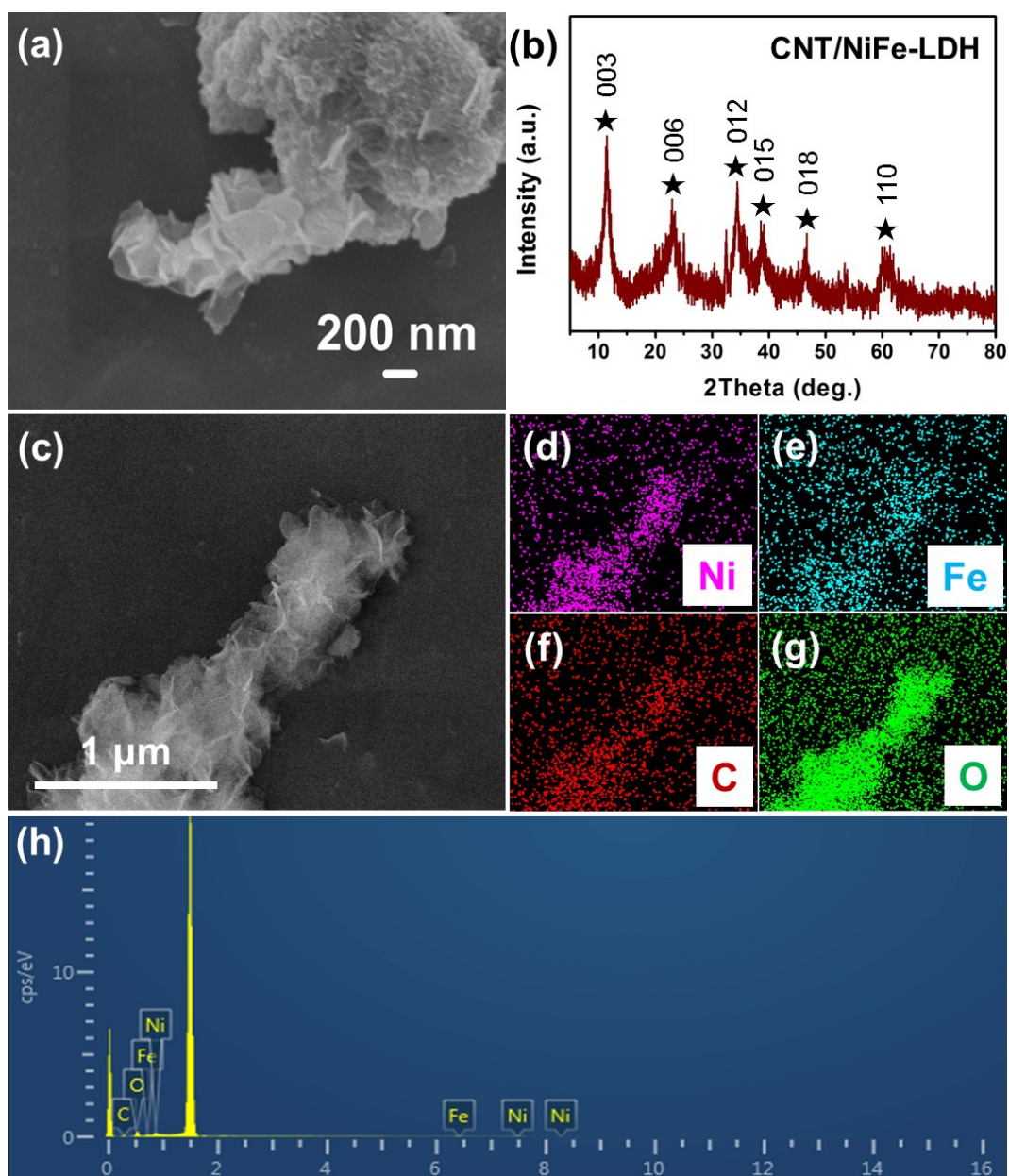


Fig. S11. (a and c) SEM images, (b) XRD pattern, and (d-h) corresponding EDS mapping images of the CNT/NiFe-LDH counterpart.

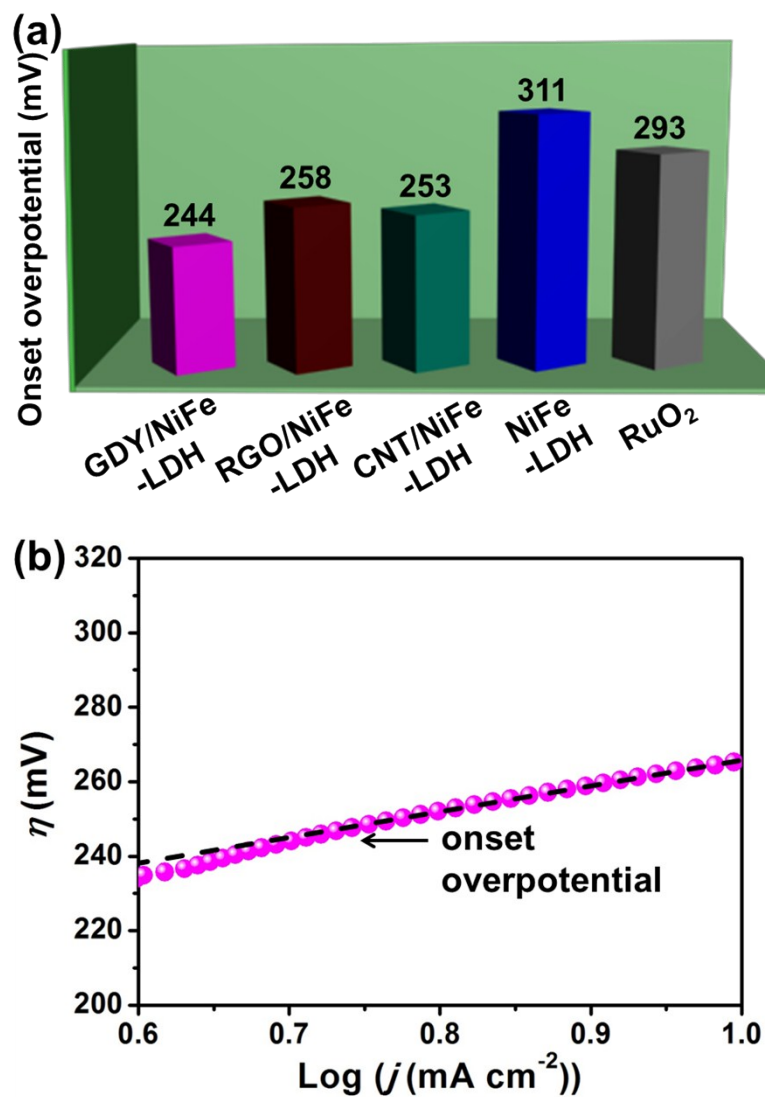


Fig. S12. (a) The onset overpotential of GDY/NiFe-LDH, RGO/NiFe-LDH, CNT/NiFe-LDH, NiFe-LDH and RuO₂. (b) The onset overpotential is determined by the potential when the Tafel plot starts to deviate from the linear region as indicated by the arrow.¹⁴

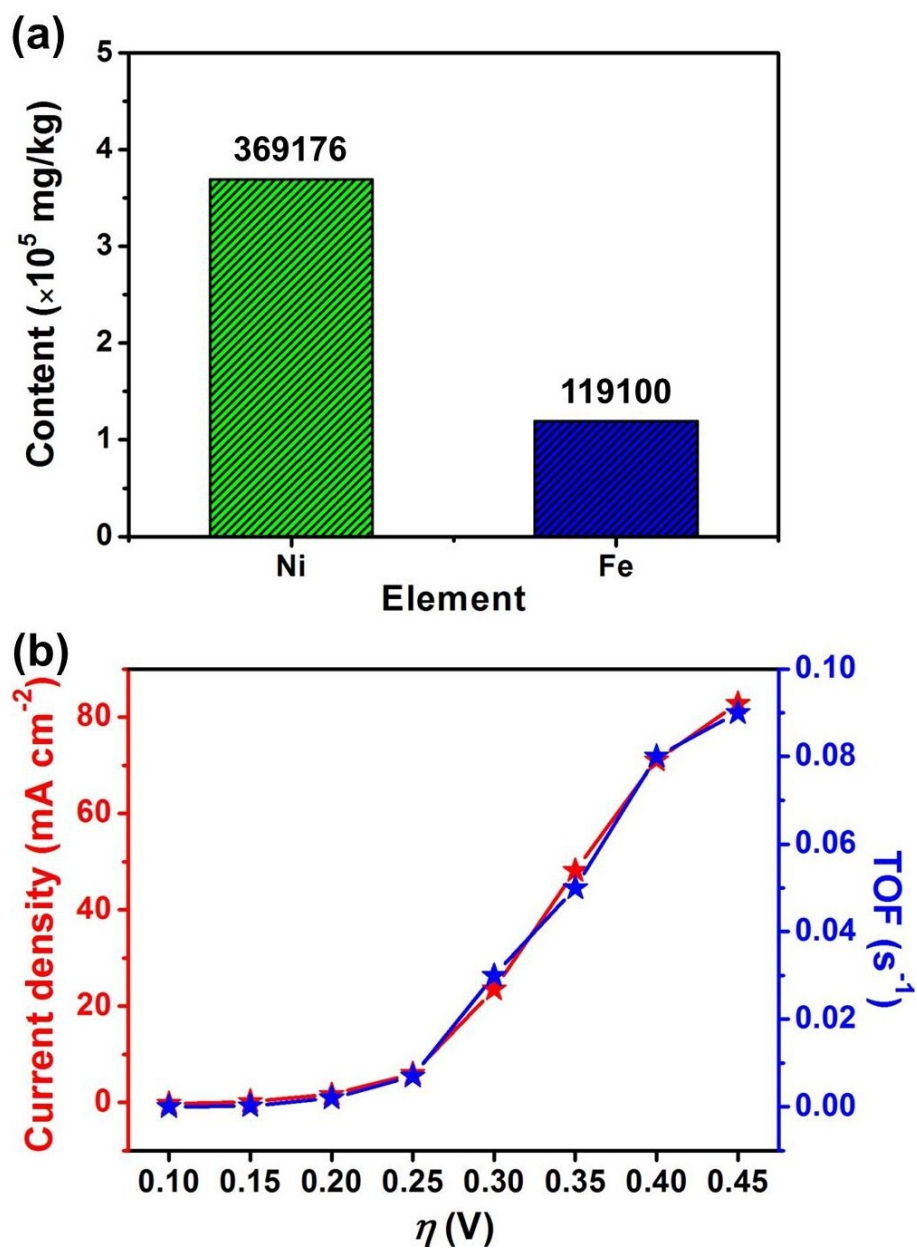


Fig. S13. (a) ICP-AES result of GDY/NiFe-LDH. (b) Current density and corresponding TOF of GDY/NiFe-LDH at different overpotential.

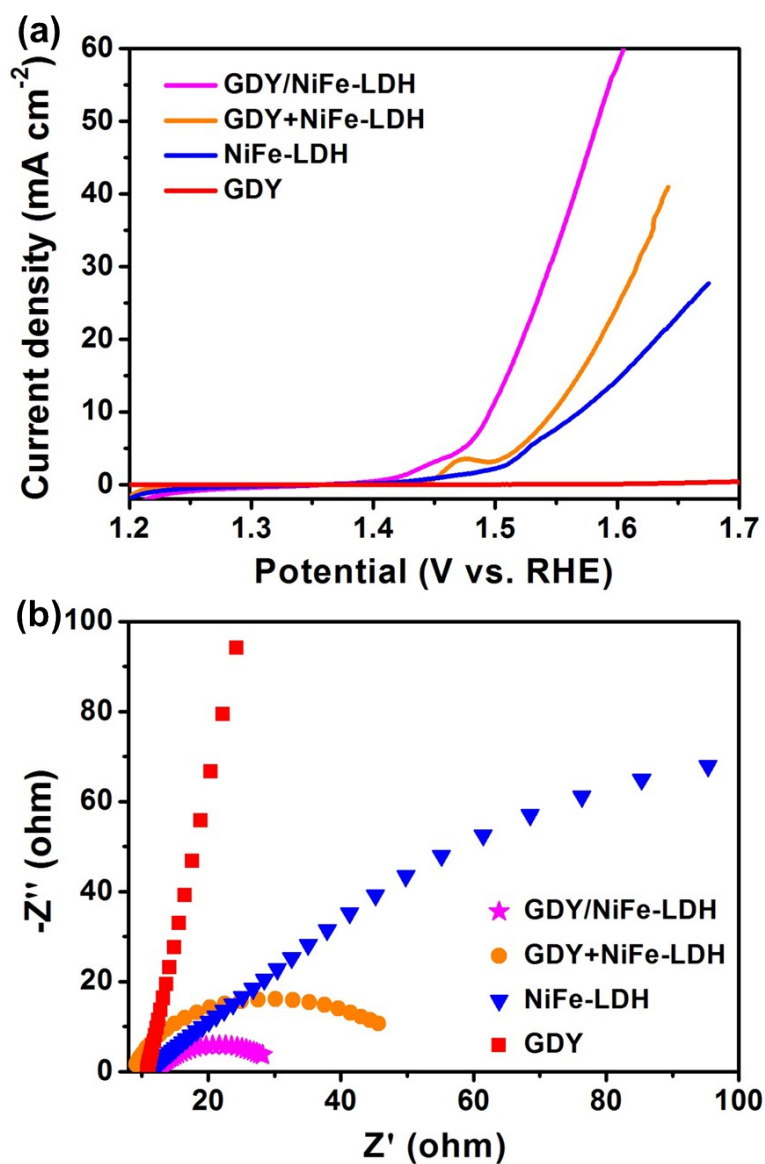


Fig. S14. (a) Polarization curves of GDY/NiFe-LDH, GDY+NiFe-LDH, NiFe-LDH and GDY electrodes. (b) Nyquist plots of samples with an overpotential of 300 mV in 1.0 M KOH.

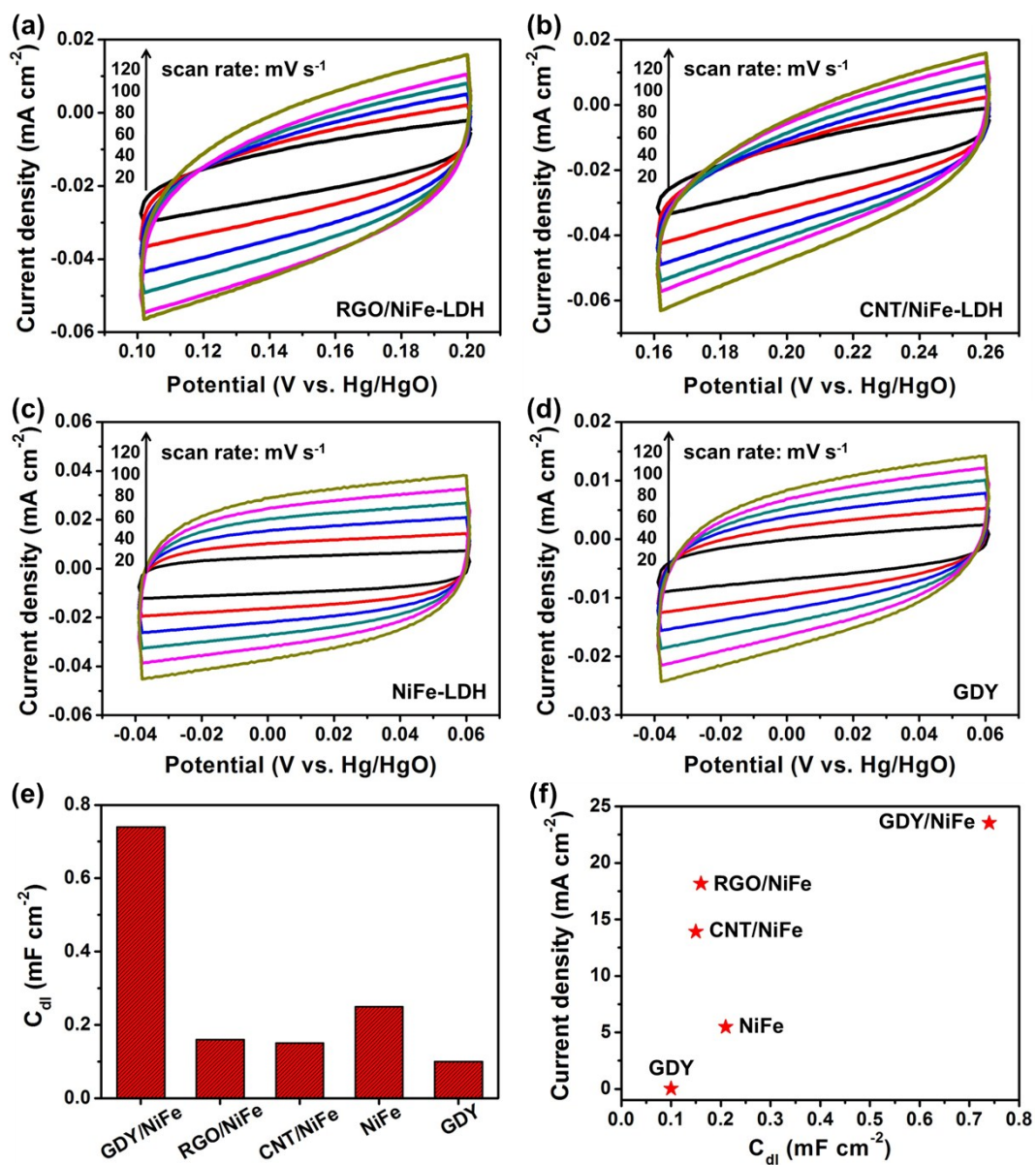


Fig. S15. CV curves of (a) RGO/NiFe-LDH, (b) CNT/NiFe-LDH, (c) NiFe-LDH and (d) GDY electrodes in 1.0 M KOH with different scan rates. (e) Double-layer capacitances and (f) current density at 300 mV overpotential plotted against C_{dl} of the samples.

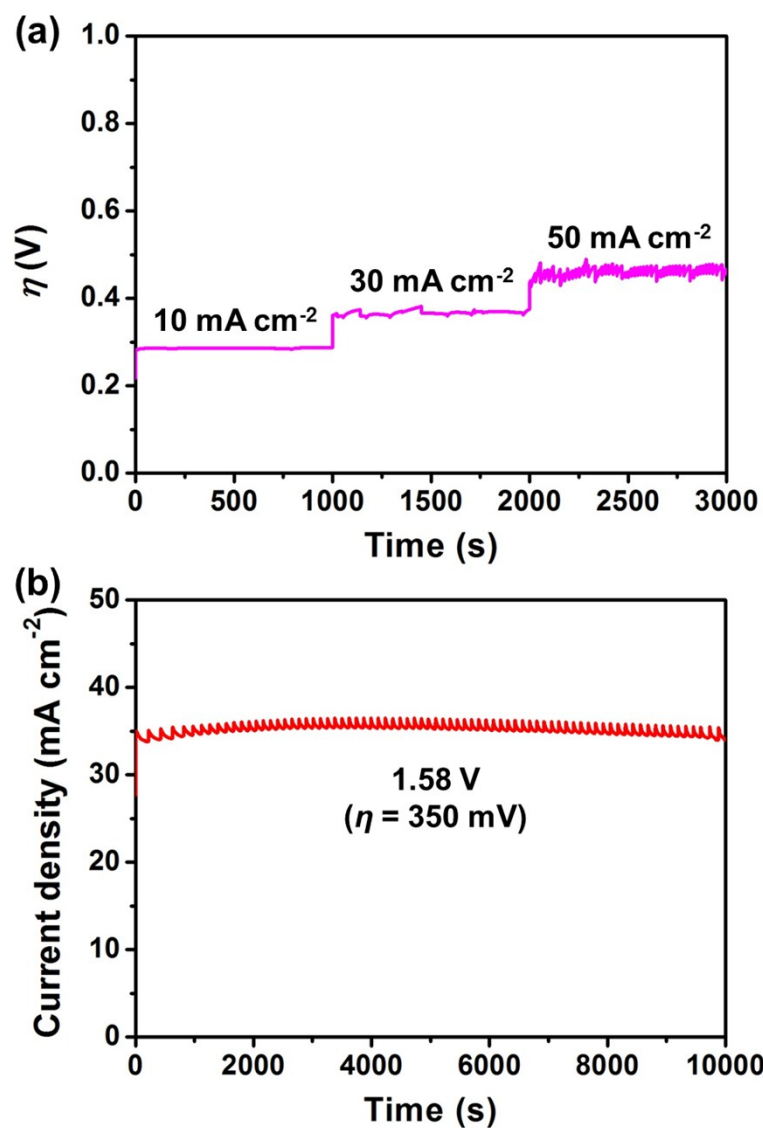


Fig. S16. (a) Multi-current process obtained with the GDY/NiFe-LDH electrode in 1.0 M KOH. The current density started at 10 mA cm⁻² and finished at 50 mA cm⁻², with an increment of 20 mA cm⁻² every 1000 s. (b) Time-dependent current density of GDY/NiFe-LDH electrode with constant overpotential of 350 mV in 1.0 M KOH.

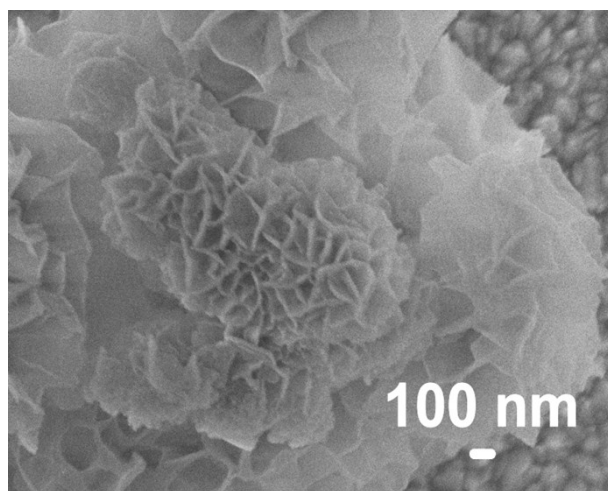


Fig. S17. SEM image of GDY/NiFe-LDH after long-term OER test in 1.0 M KOH. The background is the FTO glass substrate as the sample holder.

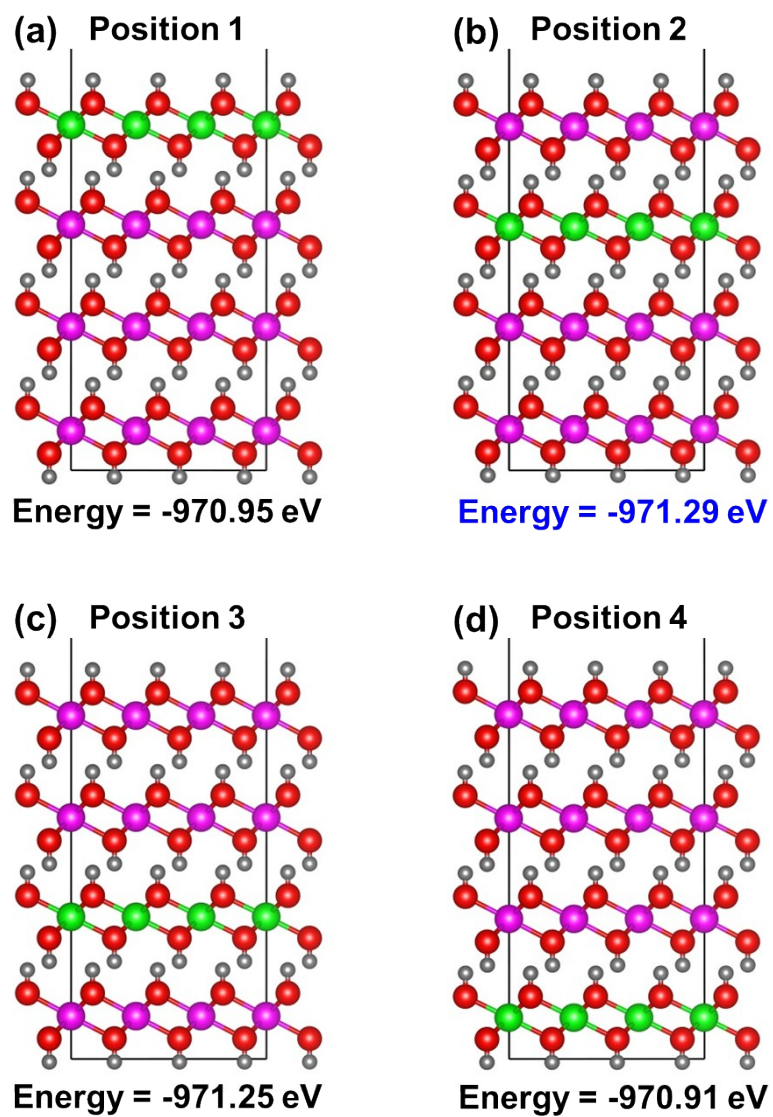
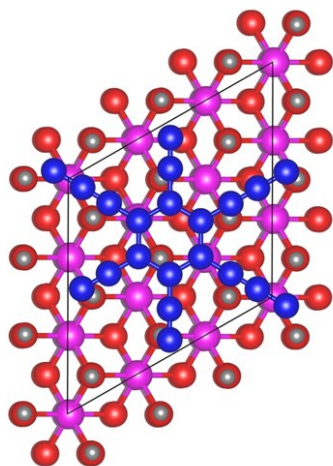
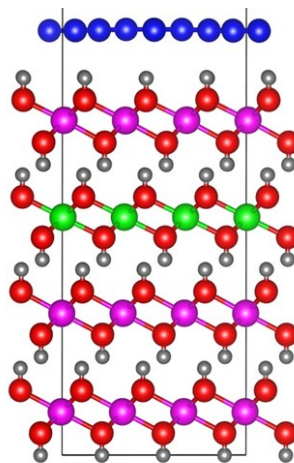


Fig. S18. Different positions of Fe (green ball) in NiFe-LDH with corresponding energies.

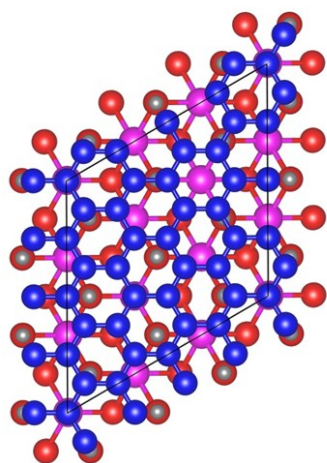
(a) Top view of
GDY/NiFe-LDH



Side view of
GDY/NiFe-LDH



(b) Top view of
RGO/NiFe-LDH



Side view of
RGO/NiFe-LDH

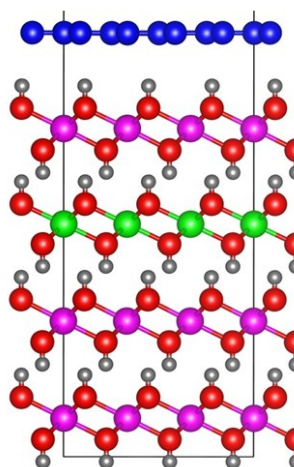


Fig. S19. Top and side views of schematic models showing (a) GDY/NiFe-LDH and (b) RGO/NiFe-LDH.

Table S1 Summary of the data for Ni 2p XPS spectrum.

	Ni 2p _{1/2} (eV)	Ni 2p _{3/2} (eV)
GDY/NiFe-LDH	872.9	855.4
RGO/NiFe-LDH	872.7	855.1
CNT/NiFe-LDH	872.6	855.1
NiFe-LDH	872.4	854.8

Table S2 The overpotentials at the current density of 10 mA cm^{-2} (η_{10}), onset overpotential, Tafel slopes, and electrochemical double-layer capacitances (C_{dl}) of the samples used for electrocatalytic OER tests in 1.0 M KOH.

Catalysts	η_{10} (mV)	Onset overpotential (mV)	Tafel slope (mV dec ⁻¹)	C_{dl} (mF cm ⁻²)
GDY/NiFe-LDH	260	244	71	0.74
RGO/NiFe-LDH	277	258	85	0.16
CNT/NiFe-LDH	285	253	97	0.15
NiFe-LDH	340	311	169	0.21
GDY	-	-	-	0.09
RuO ₂	390	293	78	-

Table S3 Comparison of the OER activity of the GDY/NiFe-LDH with reported state-of-the-art and carbon material-included OER catalysts in alkaline condition.

Catalysts	Mass loading (mg cm ⁻²)	Substrate ^a	Electrolyte	η_{10} (mV)	Ref.
GDY/NiFe-LDH	0.28	GCE	1.0 M KOH	260	This work
NiFe-NS	0.07	GCE	1.0 M KOH	290	<i>Nat. Commun.</i> 2014, 5, 4477
Ni _{0.75} V _{0.25} -LDH	0.14	GCE	1.0 M KOH	320	<i>Nat. Commun.</i> 2016, 7, 11981
Ni _{2/3} Fe _{1/3} -NS	0.25	GCE	1.0 M KOH	310	<i>ACS Nano</i> 2015, 9, 1977
Na _{0.08} Ni _{0.9} Fe _{0.1} O ₂	0.13	RDE	1.0 M KOH	260	<i>Energy Environ. Sci.</i> 2017, 10, 121
CoMn-LDH	0.14	GCE	1.0 M KOH	324	<i>J. Am. Chem. Soc.</i> 2014, 136, 16481
Ni-Co nanowire	0.3	Carbon fiber	1.0 M KOH	302	<i>Adv. Energy Mater.</i> 2017, 7, 1601492
CoNi(OH) _x	0.72	Cu foil	1.0 M KOH	280	<i>Adv. Energy Mater.</i> 2016, 6, 1501661
Exfoliated NiCo LDH	0.17	Carbon substrate	1.0 M KOH	367	<i>Nano Lett.</i> 2015, 15, 1421
FeNi ₃ N-NPs	0.35	GCE	1.0 M KOH	280	<i>Adv. Energy Mater.</i> 2016, 6, 1502585
Co ₅ Mn-LDH/MWCNT	0.28	RDE	1.0 M KOH	300	<i>ACS Appl. Mater. Interfaces</i> 2016, 8, 14527
nNiFe LDH/NGF	0.25	RDE	0.1 M KOH	337	<i>Adv. Mater.</i> 2015, 27, 4516

O-NiCoFe-LDH	0.12	RDE	0.1 M KOH	340	<i>Adv. Energy Mater.</i> 2015, 1500245
NiFe-LDH/G/Ni	2.18	Ni foam	0.1 M KOH	325	<i>J. Mater. Chem. A</i> 2015, 3, 16183
NiFe LDH/oGSH	0.25	RDE	0.1 M KOH	350	<i>J. Mater. Chem. A</i> 2015, 3, 24540

^a GCE: glassy carbon electrode

RDE: rotating disk electrode

Supporting references

- S1 Y. Xue, J. Li, Z. Xue, Y. Li, H. Liu, D. Li, W. Yang and Y. Li, *ACS Appl. Mater. Interfaces*, 2016, **8**, 31083-31091.
- S2 F. Ning, M. Shao, S. Xu, Y. Fu, R. Zhang, M. Wei, D. G. Evans and X. Duan, *Energy Environ. Sci.*, 2016, **9**, 2633-2643.
- S3 D. Higgins, P. Zamani, A. Yu and Z. Chen, *Energy Environ. Sci.*, 2016, **9**, 357-390.
- S4 L. L. Feng, G. Yu, Y. Wu, G. D. Li, H. Li, Y. Sun, T. Asefa, W. Chen and X. Zou, *J. Am. Chem. Soc.*, 2015, **137**, 14023-14026.
- S5 K. Fan, Y. Ji, H. Zou, J. Zhang, B. Zhu, H. Chen, Q. Daniel, Y. Luo, J. Yu and L. Sun, *Angew. Chem. Int. Ed.*, 2017, **56**, 3289-3293.
- S6 J. Liu, B. Cheng and J. Yu, *Phys. Chem. Chem. Phys.*, 2016, **18**, 31175-31183.
- S7 M. Zhou, L. Yan, H. Ling, Y. Diao, X. Pang, Y. Wang and K. Gao, *Appl. Surf. Sci.*, 2017, **404**, 246-253.
- S8 G. Li, Y. Li, H. Liu, Y. Guo, Y. Li and D. Zhu, *Chem. Commun.*, 2010, **46**, 3256-3258.
- S9 C. Lei, X. Zhu, B. Zhu, C. Jiang, Y. Le and J. Yu, *J. Hazard. Mater.*, 2017, **321**, 801-811.
- S10 A. R. Kumarasinghe, L. Samaranayake, F. Bondino, E. Magnano, N. Kottegoda, E. Carlino, U. N. Ratnayake, A. A. P. Alwis, V. Karunaratne and G. A. J. Amaratunga, *J. Phys. Chem. C*, 2013, **117**, 9507-9519.
- S11 B. Nagendra, K. Mohan and E. B. Gowd, *ACS Appl. Mater. Interfaces*, 2015, **7**, 12399-12410.
- S12 R. Chen, T. Zhao, J. Lu, F. Wu, L. Li, J. Chen, G. Tan, Y. Ye and K. Amine, *Nano Lett.*, 2013, **13**, 4642-4649.
- S13 H. Lu, Z. Zhu, H. Zhang, J. Zhu, Y. Qiu, L. Zhu and S. Küppers, *ACS Appl. Mater. Interfaces*, 2016, **8**, 25343-25352.
- S14 Y. Xue, Z. Zuo, Y. Li, H. Liu and Y. Li, *Small*, 2017, **13**, 1700936.